# Premature capacity loss in lead/acid batteries with antimony-free grids during cycling under constant-voltage-charging conditions
# 1. Characterization and causes of the phenomenon

H. Dietz, H. Niepraschk and K. Wiesener
*Dresden University of Technology, 01069 Dresden (Germany)*

J. Garche
*Centre for Solar Energy and Hydrogen Research, 89081 Ulm (Germany)*

J. Bauer
*V. B. Autobatterien GmbH, 30419 Hannover (Germany)*

## Abstract

Previously, premature capacity loss (PCL) has been generally interpreted as a discharge inhibition of the positive electrode. PCL has been primarily explained by changes in the structure and the properties of the grid/corrosion-layer interface, changes in the solid-state properties of non-stoichiometric $PbO_2$ in the active mass (e.g., as an increase in the electrical resistance of the particle necks), or by means of a decrease in the conductivity of gel zones in the positive plate (gel–crystal model). A special phenomenon of antimony-dependent PCL is observed under constant-voltage charging (CVC) and (subsequent) acid stratification. This effect termed as CVC–PCL differs from the original PCL phenomenon. This is because it is identified as a polarization phenomenon at the active-mass/electrolyte interface. CVC–PCL is characterized by inhomogeneous sulfation that commences in the lower regions of the electrode with residual lead sulfate increasingly remaining in the charged state. As with PCL, CVC–PCL phenomena are not caused by an antimony deficit. However, the phenomena are substantially suppressed in the presence of antimony.

## Introduction

The elimination of antimony from the grid alloy has been found to cause premature capacity loss (PCL) and shortening of the operational life of lead/acid batteries, especially if subjected to deep discharge. This so-called antimony-free effect (AFE) was frequently observed and studied but complete clarification of the interdependence between the role of antimony and mechanism of capacity loss has not yet been achieved. Though lack of antimony favours the generation of numerous structural effects and thus PCL, there are, on the other hand, sufficient examples of early capacity decay even in the presence of antimony. Therefore, in the recent literature, AFE-like phenomena of early and rapid loss of discharge capacity of the positive electrode were termed PCL [1, 2]. This effect is encouraged by:
• unfavourable cycling conditions (i.e., low current density at the beginning of recharge, high-rate overcharge and large overcharge quantities, successive high-rate discharge, deep discharge [3])

- absence of special additives such as antimony, tin and phosphoric acid [3, 4]
- high mass utilization achieved by low-rate discharge, thin electrodes, high excess of electrolyte, high acid concentration and mobility [3, 4]
- low active mass density and low plate-stack pressure [1, 5]

The occurrence of PCL is usually attributed to resistance phenomena that are located at: (i) the grid/corrosion layer and/or (ii) within the active mass. Recently, an overall concept based on a new model of the structure of the active mass has been introduced [2].

## Resistance phenomena at the grid/corrosion-layer interface

In the literature, there is considerable evidence that the PCL is caused, or associated with, changes in the structure and composition of the interphase between the grid and the corrosion layer. Insulating layers of $PbSO_4$ [6–10] and/or $\alpha$-PbO [11, 12] are found to form around the grid surface (barrier-layer model). Grid antimony counteracts this reduction of the corrosion layer by promoting the formation of a fine-crystalline and protective $PbSO_4$ layer [13–16]. In the absence of antimony, however, the reductive attack on the corrosion layer, and thus the formation of resistance-increasing $PbSO_4$ layers, becomes easier. This results in blocking of the electron-conducting $PbO_2$ paths because of a mostly incomplete re-oxidation of the $PbSO_4$ layers in the corrosion zone [9, 17–22]. Nevertheless, whether the blocking layers are the cause or the result of PCL is still under discussion. Another influence exerted by antimony is discussed with regard to the formation of $Pb_{(1-x)}Sb_xO_2$ within the corrosion layer [23]. This is a substance which, compared with $PbO_2$, is reduced at a more negative potential.

Substituting antimony by calcium also results in specific passivation phenomena at the grid/active-mass interface. This leads to high plate polarizations and poor charge acceptance. These phenomena can be avoided by adding small amounts of tin (0.2–0.6 wt.%) to the lead–calcium grid alloy and, therefore, are termed the tin-free effect.

The so-called thermopassivation observed with high-temperature drying of formed positive plates can also be prevented by tin addition to the positive electrode (i.e., by alloying, electrochemical, chemical or mechanical deposition [15, 16, 24–26]. The mode of tin action is presumed to be based on an alteration in the conductivity type (n-$PbO_n$ instead of p-$PbO_n$) and an influence on $PbO_2$ formation [10]. This means that tin causes an enlargement of the phase-width of $PbO_2$ so that the lead dioxide remains an n-type semiconductor of high conductivity even at low oxygen contents. Within the corrosion layer, mixed oxides of tin and lead of the type $Sn_{1-x}Pb_xO_2$ can be built up. The PbO formed in the presence of tin may also be disproportionated to Pb and $SnO_2$ [27]. The electrical connection is maintained by means of these conductive channels. When the grid is coated by a tin layer, a $SnO_2$–SnO layer is formed and separates the Pb phase from the $PbO_2$ phase. Because of the low diffusion coefficient of oxygen, this layer prevents the formation of a passivating PbO layer. On the other hand, the $SnO_2$–SnO layer ensures the electrical connection because of its good conductivity.

Whether the passivation that develops under charging/discharging and the passivation produced in a currentless-state (such as thermopassivation or storage passivation) have a similar mechanism has not yet been fully clarified.

Some authors assume that PCL and currentless-state passivation, e.g., thermopassivation, are separate phenomena because the nature of the phase composition of the grid/corrosion layer/active mass seems to be the only variable in the latter case

[2], and because process parameters such as sulfuric acid concentration exert a reverse influence on PCL and thermopassivation [24].

Premature losses in capacity can be also induced by a sudden cracking of the corrosion layer caused by increasing internal stress [28]. As recently shown [29] by means of electron-optical methods, the grid/active-mass interphase formed in the case of lead–antimony alloys is denser and more compact than that attained by using lead–calcium grids.

## Reversible resistance phenomena in the active mass

Many experts assume that PCL is caused by structural changes in the active mass. The latter result in impaired contact between $PbO_2$ crystals (Kugelhaufen model), changes in their intrinsic electrochemical conductivity (hydrogen-loss model), and changes in the $\alpha/\beta$-$PbO_2$ ratio, as recently reviewed by Pavlov [2].

According to the Kugelhaufen model [30–36], the positive active mass is described as a three-dimensional network of spherical $PbO_2$ particles. The properties of the contact zones between these particles (necks) are assumed to determine electrical conductivity and, thus, PCL.

Differences in dimensions concerning the particles of the active mass and their connecting necks will lead to differences in surface tensions that, in turn, will effect different electrochemical potentials for the active-mass particles and necks. For large particles, the potential difference between the particle and the neck is small. This means that the neck zone is diminished even after a short period of discharge and, therefore, further discharge processes are blocked. For smaller mass particles, a higher potential difference is observed. The decreases in the area and the electron conductivity of the neck zones are reversible by washing, drying, open-circuit stand, as well as by the addition of tin [4].

In summary, the Kugelhaufen model enables PCL to be described as 'relaxable insufficient mass utilization' (RIMU) of the positive electrode under unfavourable cycling conditions and in the absence of antimony.

## Gel–crystal model of the positive electrode

Pavlov [2] has proposed a new model of the structure of the positive electrode. This views the active mass and the corrosion layer as a gel–crystal system. This approach is based on the assumption that an optimal ratio of electron-conducting crystal zones and proton-conducting gel zones is necessary to reach maximum capacity, and that the concentration of the gel zones determines capacity and PCL. The beneficial effect of antimony has been explained by its ability to improve the conductivity of the gel zones, and to decrease the critical mass density below which PCL develops.

In industrial operations of lead/acid batteries, a number of PCL phenoma, that are observed if the grid antimony is replaced by calcium, cannot be explained by the usual AFE or PCL phenomena according to the above three models. In most cases, these effects take place gradually and also earlier than the original PCL. Analogously to AFE or RIMU, these phenomena are not strictly connected to the lack of antimony. In fact, they occur in a less pronounced form in the presence of antimony. These phenomena occur at increased overvoltage of the negative electrode, and at extremely

low charge input (overcharge <5%) when charging with low constant-voltage and at (subsequent) acid stratification [22, 37, 38].

Such an antimony-dependent manifestation of PCL under constant-voltage-charging conditions (CVC–PCL) is also observed during cycling of automotive batteries according to DIN 43539/2 [39]. Therefore, the objectives of the work reported here are: (i) to describe CVC–PCL phenomena under acid-stratification conditions and under the influence of antimony deficiency; (ii) to determine the cause(s) of these phenomena; (iii) to study and propose measures for prevention of CVC–PCL.

## Experimental

In order to study the antimony-dependent CVC–PCL 2 V/36 Ah single cells with 3 positive and 4 negative plates were subjected to a weekly cycle test according to DIN 43539/2. The grids used for the positive electrodes were: (i) Pb–0.09wt.%Ca–0.3wt.%Sn and (ii) Pb–2.5wt.%Sb. The grid alloy of the negative plate was always Pb–0.09wt.%Ca–0.3wt.%Sn. The mass composition of the positive and negative electrodes corresponded to usual specifications. The total ratio of the positive to negative active material was 1.09. Both types of positive electrodes contained the same amount of active material. The positive electrodes were enveloped in Daramic separators. The amount of electrolyte was 600 cm$^3$ $H_2SO_4$ per cell. The acid did not contain any additives. A container-formation procedure was conducted in acid of 1.23 sp. gr. with subsequent correction in acid density to 1.28 sp. gr. before testing.

After cycles of 0, 2, 4 or 6 weeks and at the failure cycle (after having reached the DIN limit), one cell was subjected to the tests described below. For ensuring a definite initial state, the elements, which had sometimes been stored for a longer time, were discharged once at $I_{20}$ until 1.75 V/cell, and then charged at $2 \times I_{20}$ until 2.47 V/cell and, subsequently, for 5 h at 2.47 V/cell.

The following measurements were performed:

(i) Determination of electronic resistance by means of dynamic current/voltage measurements and current measurements that were performed at a constant potential difference of 50 mV with the aid of gilded copper stamps (see Fig. 1). These tests were carried out on dry plates after watering and drying at 80 °C for 12 h.

(ii) *In situ* resistance measurements (by means of an interruption technique) at the end of the discharge.

(iii) Determination of Ah capacity ($5 \times I_{20}$ to 1.67 V).

(iv) Potential and current measurements during *I/U*-recharging ($5 \times I_{20}$ or 2.47 V for 5 h) after previous discharging according to DIN.

(v) Chemical analysis of $PbO_2$ and $PbSO_4$.

## Results and discussion

### Ah-capacity measurements

The positive 12 Ah electrodes taken from weekly cycling were discharged by a constant current of $5 \times I_{20}$ until an end-of-discharge voltage of 1.67 V was reached. In this way, the capacity, $K_4$, was determined. The measured capacity values were referred to the initial capacity before cycling. The data are presented in Fig. 1. All electrodes subjected to a cycling according to DIN 43539/2 exhibited a distinct loss in capacity during the testing process. In comparison with positive electrodes using lead–antimony alloys those based on a lead–calcium grids showed a greater decrease of capacity. This effects an earlier decline to below the DIN limit of 6 Ah.

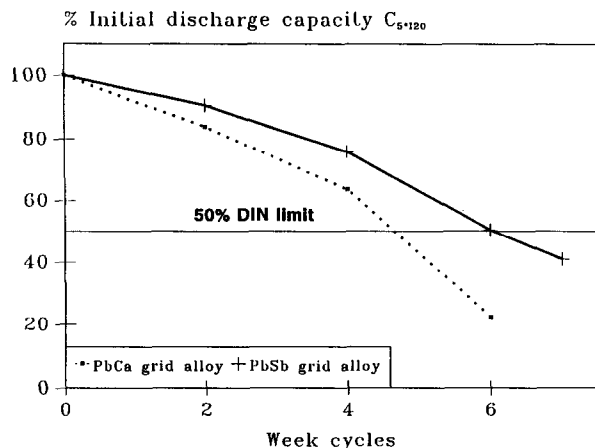% Initial discharge capacity $C_{5-120}$



Fig. 1. Loss of initial discharge capacity of 12 Ah positive electrodes with different grid alloys during cycling according to DIN 43539/2 (weekly cycle test). (a) Pb–Sb(+)/Pb–Ca(−); (b) Pb–Ca(+)/Pb–Ca(−).
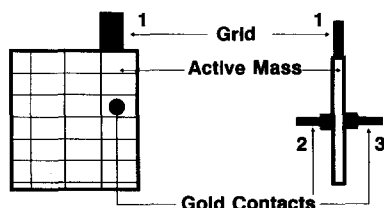


Fig. 2. Arrangement for resistance determination of dry positive electrodes. Measuring points: 1–2 (grid/active material); 2–3 (active material/active material).

*Resistance measurements on dried electrodes*

To characterize the cause of failure, measurements of the electronic resistance were performed at different locations on dried positive electrodes. The apparatus used is shown in Fig. 2. The contacts 1–2 served to measure the resistance of the grid/active-mass interface. By means of the contacts 2–3, the resistance of the active mass alone was measured. The stamp pressure was 10 kPa cm$^{-2}$. With this procedure, the following questions should be answered:

(i) Is it feasible to determine increases in resistance that cause PCL?

(ii) Where does the increase in resistance occur?

(iii) What is the type of the resistors (semiconductors or ohmic resistors)?

In order to localize the regions where increase in resistance occurs, the current–voltage characteristic between the grid/active-mass or active-mass/active-mass contacts of charged positive electrodes with positive electrodes with lead–calcium grids were measured for electrodes that had failed the weekly tests. This characteristic was compared with that for a thermopassivated reference electrode.

The example of the thermally-dried electrode (curves a and b, Fig. 3) clearly demonstrates a significant increase in resistance between the grid and the active mass compared with the resistance of the active mass. This illustrates the capacity-limiting influence of the grid/active-mass interface.
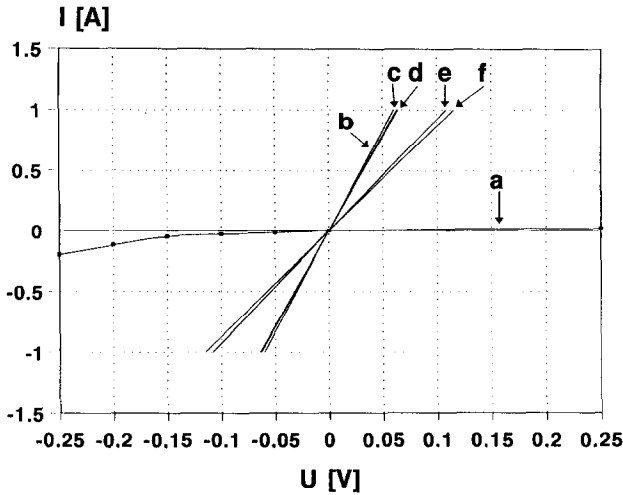
Fig. 3. Potentiodynamically recorded current–potential curves for dry positive electrodes with lead–calcium grids. Curves a and b: 3 Ah reference electrode subjected to thermal drying (170 °C for 2 h); curves c to f: 12 Ah electrodes in cycle no. 6. Resistance: (a), (d), (f)–grid/active material; (b), (c), (e)–active material/active material. Measuring location: (c), (d)–upper part, (e), (f)–lower part of the plate.

The thermally-produced passivation layer is characterized by a transition zone between two semiconductors or between the metal and a semiconductor; these differ in their mode of conductivity (p–n transition). The thermal treatment does not, however, effect any increase in the resistance of the active mass.

By contrast, the resistance measurements carried out on cycled antimony-free electrodes (curves c to f, Fig. 3) demonstrate that:
- only ohmic resistances are found
- the grid/active-mass resistance does not act as a capacity-determining element because of the comparable values of the contact resistances at the grid/active-mass and the active-mass/active-mass
- relatively high resistance values are found in the lower regions of the electrodes (curves e and f, Fig. 3)

## Interruption method for resistance measurement during discharge

To eliminate artefacts on dry electrodes caused by the possible formation of layers during the drying process, measurements were carried out *in situ* by applying the interruption method. Oscillographic recorded voltage versus time curves of fresh electrodes (week cycle: 0) did not differ from those recorded with electrodes that had failed (week cycle: 6). All the electrodes tested showed normal ohmic resistance behaviour. This is in agreement with the results derived from resistance measurements of dried electrodes.

## Determination of resistance distribution

The local resistance distribution was determined by measuring the resistance of the active mass (Fig. 2, contacts 2–3) of dried $PbO_2$ electrodes at different locations

with screen-like distribution (about 45 measuring points). Figure 4 illustrates the changes in the resistance distribution of positive electrodes as a function of cycle number. The lugs of the electrodes are marked in the relief representation. It can be concluded that: (i) at week cycle (WC) zero, there are no significant differences in resistance distribution; (ii) at week cycle = 6, the resistance of the active mass is substantially increased in the lower regions, less changed in the middle parts, but least increased in the upper zones of the positive electrode; (iii) the effect of increasing resistance is more pronounced for electrodes having lead–calcium alloys than that for electrodes with lead–antimony grids.

The data obtained from chemical analyses confirm in an unequivocal way that the increase in resistance of the active mass correlates with an increase in the $PbSO_4$ concentration. Sulfation begins in the lower electrode region. With further cycling, the middle parts of the charged positive electrode also remain in a permanently sulfated state (see Table 1).

Measurements of acid density were carried out to study the causes of the lowered chargeability. Table 2 shows that there is substantial acid stratification at the beginning
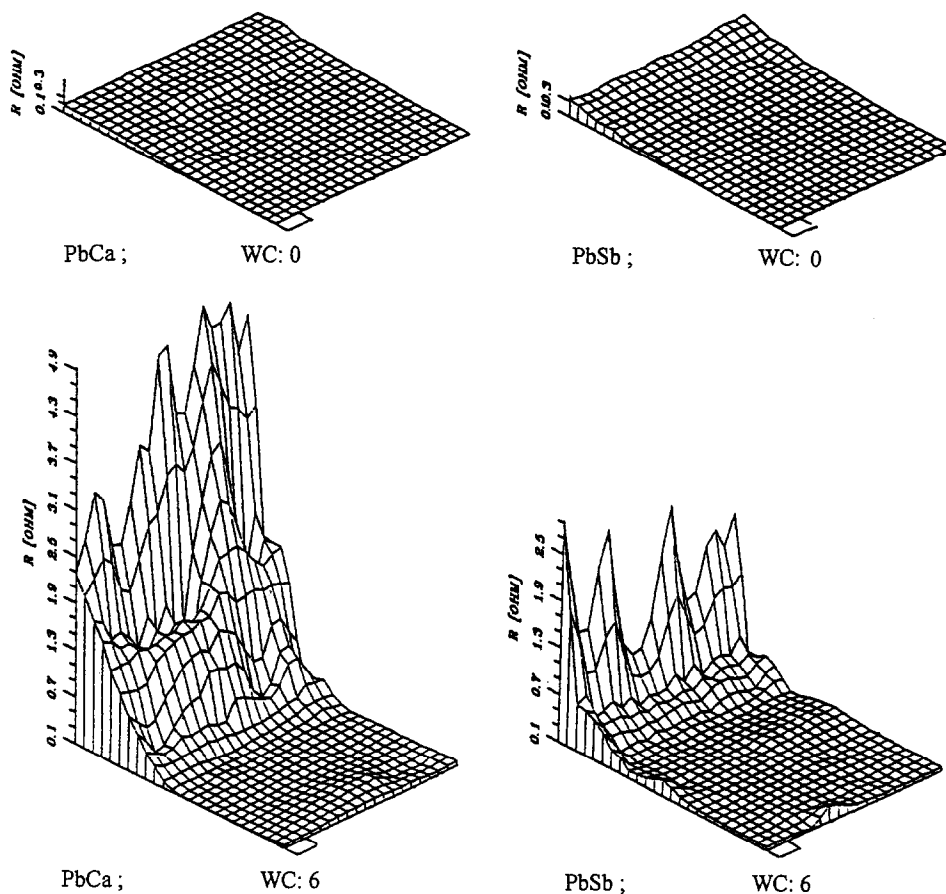


Fig. 4. Local distribution of active mass resistance of DIN-charged positive electrodes (Fig. 2; measuring points 2–3) as a function of weekly cycle number and positive grid alloy composition.

TABLE 1

Amounts of $PbO_2$ and $PbSO_4$ in active mass of positive electrodes with lead–calcium grids. Dependence on cycle number and sampling position[a]

| Week cycle | Sampling position | wt.% $PbO_2$ | wt.% $PbSO_4$ |
|---|---|---|---|
| 0 | Top | 96 | 6 |
| | Middle | 91 | 9 |
| | Bottom | 86 | 11 |
| 2 | Top | 88 | 5 |
| | Middle | 93 | 7 |
| | Bottom | 54 | 47 |
| 4 | Top | 93 | 8 |
| | Middle | 93 | 8 |
| | Bottom | 54 | 47 |
| 6 | Top | 93 | 4 |
| | Middle | 79 | 19 |
| | Bottom | 61 | 40 |

[a]State: DIN charged.

TABLE 2

Measurements of acid density in automotive batteries after 2nd weekly cycle

| $\rho$ (g cm$^{-3}$) | | |
|---|---|---|
| | Pb–Ca | Pb–Sb |
| At the top | 1.25 | 1.27 |
| At the bottom | 1.32 | 1.30 |

of cycling. This seems to be primarily responsible for the inhomogeneous distribution of resistance and sulfate concentration on the plate surface.
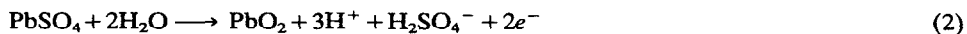
Increasing acid concentration at the lower plate region leads to an elevation of the velocity of the self-discharge reaction (eqn. (1)):
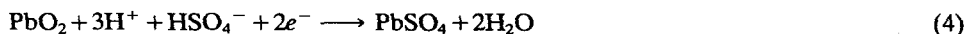
$$PbO_2 + H_2SO_4 \longrightarrow PbSO_4 + H_2O + \tfrac{1}{2}O_2 \tag{1}$$

This causes the formation of coarse $PbSO_4$ crystals because the current strength is relatively low (i.e., a low nucleation rate) in comparison with that of the external discharge.

In addition, an acid-concentration cell is formed between the upper and the lower plate regions so that the following reactions take place:

(i) at top:

$$PbSO_4 + 2H_2O \longrightarrow PbO_2 + 3H^+ + H_2SO_4^- + 2e^- \tag{2}$$

$$H_2O \longrightarrow \tfrac{1}{2}O_2 + 2H^+ + 2e^- \tag{3}$$

(ii) at bottom:

$$PbO_2 + 3H^+ + HSO_4^- + 2e^- \longrightarrow PbSO_4 + 2H_2O \tag{4}$$

As a result of eqns. (1) and (4), an increasing amount of granular, crystalline $PbSO_4$ grows in the lower electrode regions. To oxidize this modification to $PbO_2$, higher

charging voltages are required. Further details on the phenomena that occur in acid-concentration cells are under investigation [40].

Figure 5 shows the positive and negative potentials versus $Hg/HgSO_4$ and the current during recharging according to DIN. In the first stage of charging with constant current the main reaction at the positive electrode is the oxidation of $PbSO_4$ to $PbO_2$. The state of the electrode is characterized by the height and the length of the potential plateau obtained. The increase in potential position height with increasing number of cycles can be explained by an increasing polarization during the charging process. From the length of the potential plateau with respect to time, information can be gathered about the quantity of the positive active mass that can be charged under these conditions. If the positive electrode is nearly full charged or the polarization for the $PbO_2$ formation is too high to enable further oxidation of $Pb^{2+}$, the positive potential rises until the voltage limit of 2.47 V/cell comes into force. At this stage, the charging currents decrease and oxygen evolution commences. On one hand, the voltage limit restricts the electrolyte decomposition but, on the other hand, it prevents the oxidation of $PbSO_4$ (a charging problem) at a cell voltage of, or less, than 2.47 V.
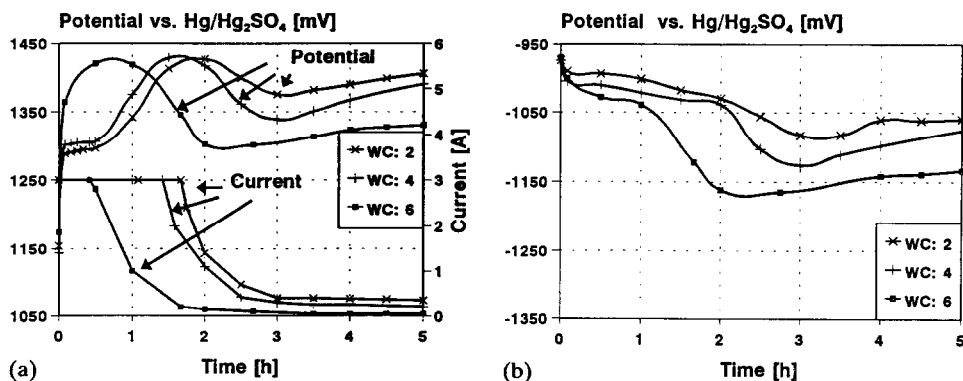


Fig. 5. Current–potential behaviour of positive and negative electrodes with lead–calcium grids vs. time at recharge. DIN 43539/2 cycling.
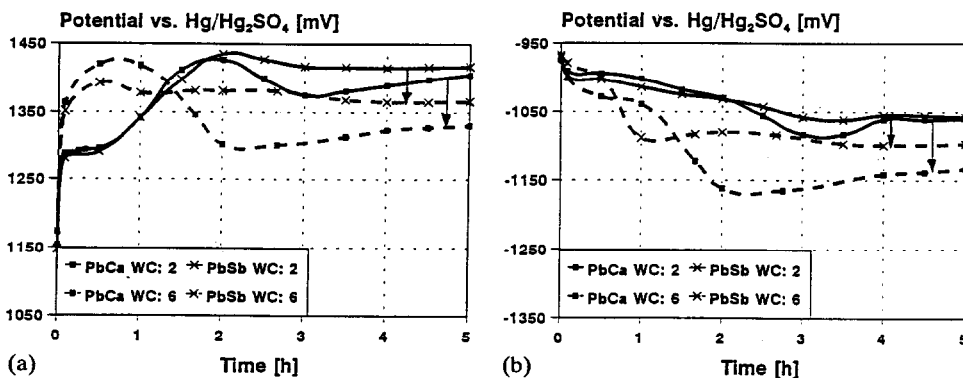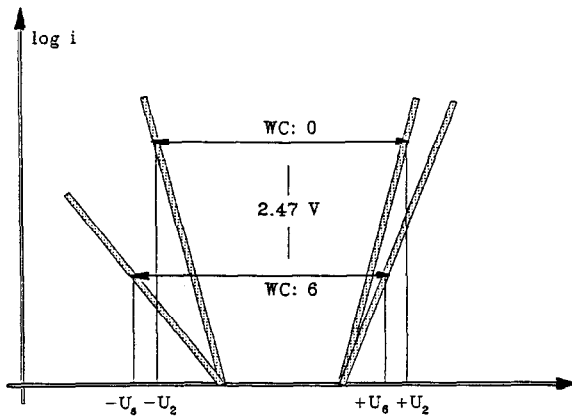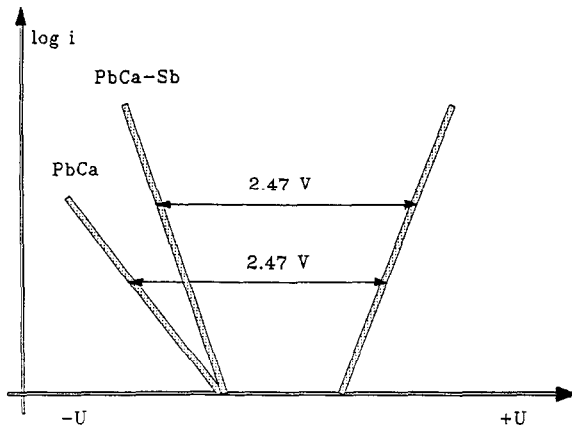


Fig. 6. Potential of positive and negative electrodes vs. time at recharge during DIN 43539/2 cycle. Dependence on cycle number and positive grid alloy composition.

(a)

(b)

Fig. 7. Model of the current input at recharge of (2 V) lead/acid cells according to DIN 43539/ 2. Dependence on: (a) cycle number; (b) antimony poisoning at the negative electrode.

From Fig. 5, it is also seen from the very beginning of recharge that, with proceeding weekly cycles, both the positive and negative electrodes become more and more polarized. Thus, the voltage limit and the beginning of the current decline are increasingly achieved earlier.

There is another important phenomenon. With proceeding week cycle number, the potentials of both the positive and negative electrodes, as well as the currents at the middle and end of charging, become more and more negative. As a result of both effects, the coulombic input at recharge is reduced by an increasing extent. This potential shift towards negative values is lowered in the presence of antimony seen in Fig. 6.

Due to increasing antimony poisoning of the negative plate (week cycle = 6), hydrogen evolution starts earlier and at more positive potentials. This leads to an elevation of the charging potential of the positive electrode under constant-voltage charging and to better chargeability compared with electrodes with antimony-free grids.

Thus, antimony partially compensates for the trend of the potential shift towards more negative values.

A simple model for the influence of the cycle number and the role of antimony on the actual potential values of both electrodes at the end of recharging under constant-voltage procedures is presented in Fig. 7. As the potential shift is observed to be directed towards negative values, the negative electrode appears to be more polarized than the positive counterpart. This appears to account for the phenomenon (Fig. 7(a)). The beneficial effect of antimony poisoning at the negative electrode in counteracting the potential shift to a negative direction is demonstrated in Fig. 7(b).

## Conclusions

1. A special phenomenon of antimony-dependent PCL (termed as CVC–PCL) occurs under cycling conditions that are based on low constant-voltage recharging, low overcharge input and (subsequent) acid stratification. This has been observed during weekly cycle testing according to DIN 43539/2.

2. The above effect has been identified as a polarization phenomenon at the active-mass/electrolyte interface of the positive electrode. It is characterized by an inhomogeneous sulfation that commences in the lower regions of the electrode. Lead sulfate builds up in the charged state. CVC–PCL differs from the original phenomenon of PCL (AFE, RIMU or passivation) which is located between the grid and the active mass and does not include incomplete charging and residual sulfation.

3. The CVC–PCL effect has been found to be primarily caused by acid stratification, because differences in acid density of substantially more than 0.07 sp. gr. have been observed between the top and bottom of the electrode. It has been concluded that the structural properties of the negative electrode, the mass ratio of positive to negative electrodes and, in particular, antimony all affect the shift in potential of the positive electrode towards negative values. This, in turn, lowers the chargeability of the positive electrode under constant-voltage charging. From the potential shift, it can be derived that the negative electrode controls the actual potential values of both electrodes.

4. Analogous to observations of PCL, CVC–PCL phenomena are not caused by an antimony deficit, but are substantially suppressed in the presence of antimony. Antimony exerts a beneficial influence during recharge. Hence, the decrease in hydrogen overvoltage due to antimony deposition at the surface of the negative electrode leads both to a higher charging potential of the positive electrode and to early gassing and, as a result, to less acid stratification.

5. Additional tests will be necessary to: (i) elucidate the full mechanism and causes of CVC–PCL, including an understanding of the controlling function of the negative electrode on the potential shift that is observed when charging at low constant voltages; (ii) determine methods for diminishing the CVC–PCL effect.

## References

1 A.F. Hollenkamp, J. Power Sources, 36 (1991) 567.
2 D. Pavlov, J. Power Sources, 42 (1993) 345.
3 E. Meissner and E. Voss, J. Power Sources, 33 (1991) 231.
4 E. Meissner and H. Rabenstein, J. Power Sources, 40 (1992) 157.
5 T.G. Chang in K.R. Bullock and D. Pavlov (eds.), Proc. Symp. Advances in Lead–Acid Batteries, Vol. 84–14, The Electrochemical Society, Pennington, NJ, USA, 1984, p. 86.

6  S. Tudor, A. Weisstuch and S. H. Davang, *Electrochem. Technol.*, 5 (1967) 21.
7  I.K. Gibson, K. Peters and F. Wilson, in J. Thompson (ed.), *Power Sources 8*, Academic Press, London, 1981, p. 565.
8  G. Kawamura, S. Mochizuki and A. Komaki, *Prog. Batteries Solar Cells*, 4 (1982) 167.
9  A. Kita, Y. Matsumaru and J. Yamashita, *Yuasa-Jiho*, 58 (1985) 7.
10  J. Yamashita, H. Yufu and Y. Matsumaru, *J. Power Sources*, 30 (1990) 13.
11  H.K. Giess, in K.R. Bullock and D. Pavlov (eds.), *Proc. Symp. Advances in Lead–Acid Batteries*, Vol. 84-14, The Electrochemical Society, Pennington, NJ, USA, 1984, p. 241.
12  A. Kita, Y. Katsumaru, M. Shimpo and H. Nakashima, in L. Pearce (ed.), *Power Sources 11*, Leatherhead, Surrey, UK, 1986, p. 31.
13  J. Garche, *Habilitation Thesis*, Technical University Dresden, 1982.
14  J. Garche, E. Voss, R.F. Nelson and D.A.J. Rand, *J. Power Sources*, 36 (1991) 405.
15  H. Döring, J. Garche, W. Fischer and K. Wiesener, *J. Power Sources*, 28 (1989) 367.
16  H. Döring, J. Garche, H. Dietz and K. Wiesener, *J. Power Sources*, 30 (1990) 41.
17  Z. Takehara and K. Kanamura, *Bull. Chem. Soc. Jpn.*, 60 (1987) 1567.
18  Z. Takehara and K. Kanamura, *J. Electrochem. Soc.*, 134 (1987) 13.
19  Z. Takehara and K. Kanamura, *J. Electrochem. Soc.*, 134 (1987) 1604.
20  Z. Takehara, K. Kanamura and K. Kawanami, *J. Electrochem. Soc.*, 136 (1989) 620.
21  Z. Takehara, *J. Power Sources*, 30 (1990) 55.
22  E.M. Valeriote, A. Heim and M.S. Ho, *J. Power Sources*, 33 (1991) 187.
23  D. Pavlov and B. Monachov, *Unesco Expert Workshop, Theory and Practice of the Lead/Acid Sytem, Gaussig, Germany, Apr. 2–5, 1991*.
24  K. Takahashi, H. Yasuda, N. Takami, S. Horie and Y. Suzui, *J. Power Sources*, 36 (1991) 451.
25  R.F. Nelson and D.M. Wisdom, *J. Power Sources*, 33 (1991) 165.
26  K. Takahashi, N. Hoshihara, H, Yasuda, T. Ishii and H. Jimbo, *J. Power Sources*, 30 (1990) 23.
27  M. Terada, S. Saito, T. Hayakawa and A. Komaki, *Prog. Batteries Solar Cells*, 8 (1989) 214.
28  I.K. Gibson, K. Peters and F. Wilson, in J. Thompson (ed.), *Power Sources 8*, Academic Press, London, 1981, p. 577.
29  A.F. Hollenkamp, K.K. Constanti, A.M. Huey, M.J. Koop and I. Apăteanu, *J. Power Sources*, 40 (1992) 125.
30  U. Hullmeine, E. Voss and A. Winsel, *J. Power Sources*, 25 (1989) 27.
31  E. Voss, U. Hullmeine and A. Winsel, *J. Power Sources*, 30 (1990) 33.
32  E. Voss and A. Winsel, *Yuasa-Jiho*, 68 (1990) 4.
33  A. Winsel, E. Voss and U. Hullmeine, *J. Power Sources*, 30 (1990) 209.
34  A. Winsel, E. Voss und U. Hullmeine, *DECHEMA-Monogr.*, 121 (1990) 209.
35  W. Borger, U. Hullmeine, H. Laig-Hörstebrock and E. Meissner, in T. Keily and B.W. Baxter (eds.), *Power Sources 12*, Int. Power Sources Symp. Committee, Leatherhead, UK, 1988, p. 131.
36  U. Hullmeine, E. Voss and A. Winsel, *J. Power Sources*, 30 (1990) 99.
37  W.G. Sunu and B.W. Burrows, in J. Thompson (ed.), *Power Sources 8*, Academic Press, London, 1981, p. 601.
38  E. Voss, *J. Power Sources*, 7 (1982) 343.
39  G. Richter, *J. Power Sources*, 42 (1993) 231.
40  A. Preuße, H. Dietz and K. Wiesener, *Ext. Abstr., Proc. Int. Conf. on Lead/Acid Batteries: LABAT '93, St. Konstantin, Varna, Bulgaria, June 7–11, 1993*, Abstr. No. 25.